

# Timing and structural controls on skarn-type and vein-type mineralization at the Xitian tin-polymetallic deposit, Hunan Province, SE China

Miao He<sup>1,2</sup> · Quanlin Hou<sup>1,2</sup> · Qing Liu<sup>1,2</sup> · Jiheng Zhang<sup>1,2</sup> · Jinfeng Sun<sup>1,2</sup> ·  
Shichong Wu<sup>3</sup> · Haofeng Zhu<sup>3</sup>

Received: 6 February 2017 / Revised: 2 May 2017 / Accepted: 16 August 2017 / Published online: 31 August 2017  
© Science Press, Institute of Geochemistry, CAS and Springer-Verlag GmbH Germany 2017

**Abstract** Xitian tin-polymetallic deposit, located in the eastern Hunan Province, SE China, hosts quartz vein and skarn in the contact zone between carbonate and two stages granites. Critical geodynamic questions for South China are whether different types of mineralization form in the same time and how the magmatism–tectonic system controls the ore-forming process. Based on the distribution of the orebodies, six cassiterite samples from different types of mineralization are collected for dating. In-situ LA-MC-ICP-MS U–Pb isotopic data yielded concordia low intercept ages between 154 and 157 Ma, indicating that different types of mineralization belong to the same magmatism–mineralization system. Coupled with the study of the kinematic indicators, it suggests that the structural control of the wall rocks constrain the types of mineralization. These results provide further evidence of a close temporal link between the structure and the tin-polymetallic mineralization in Xitian deposit. Considering the structure in the district, granite dome plays an important role in the ore-forming process. The age and structural signatures in Xitian deposit are the response to the subduction of Pacific Plate.

**Keywords** LA-MC-ICP-MS U–Pb dating · Structure control · Tin-polymetallic deposit · SE China

## 1 Introduction

The Nanling Range, located in the southern part of the South China Block, is famous for the numerous W–Sn deposits that are closely associated with voluminous Mesozoic granitic magmatism (Wang et al. 2014b; Zhang et al. 2015; Zhao and Zhou 2015). Extensive studies have been performed that reveal the genetic relationship between ore deposits and granites in the Nanling Range (Chen et al. 2013b; Liu et al. 2007; Ma et al. 2008; Wang et al. 2014a; Yuan et al. 2011). The peak of mineralization in the Nanling Range is deemed to be Yanshanian according to massive geochronology studies of the tin-polymetallic deposits (Guo et al. 2011; Hu and Zhou 2012; Mao et al. 2008; Peng et al. 2006). However, with increasing geochronology studies in the Nanling Range recently, the Indosinian tin-polymetallic mineralization that is genetically related to Indosinian granites is also widespread and more common than previous thought (Cai et al. 2006; Liu et al. 2008b; Wu et al. 2012a; Yang et al. 2009; Zhang et al. 2015). Additionally, based on the distribution of the skarn-type orebodies, which are spread in the outer contact zone of the Indosinian granites, the potential of Indosinian mineralization in the Xitian deposit attracts a group's attention (Cai et al. 2006; Liu et al. 2016; Mao et al. 2013; Zhang et al. 2015). The Xitian tin-polymetallic deposit located at the central of the Nanling Range is one of the representatives (Fig. 1). It has multi-phase intrusions and complex types of mineralization. However, previous geochronology studies have revealed that rocks of different episodes cannot be adequately classified by

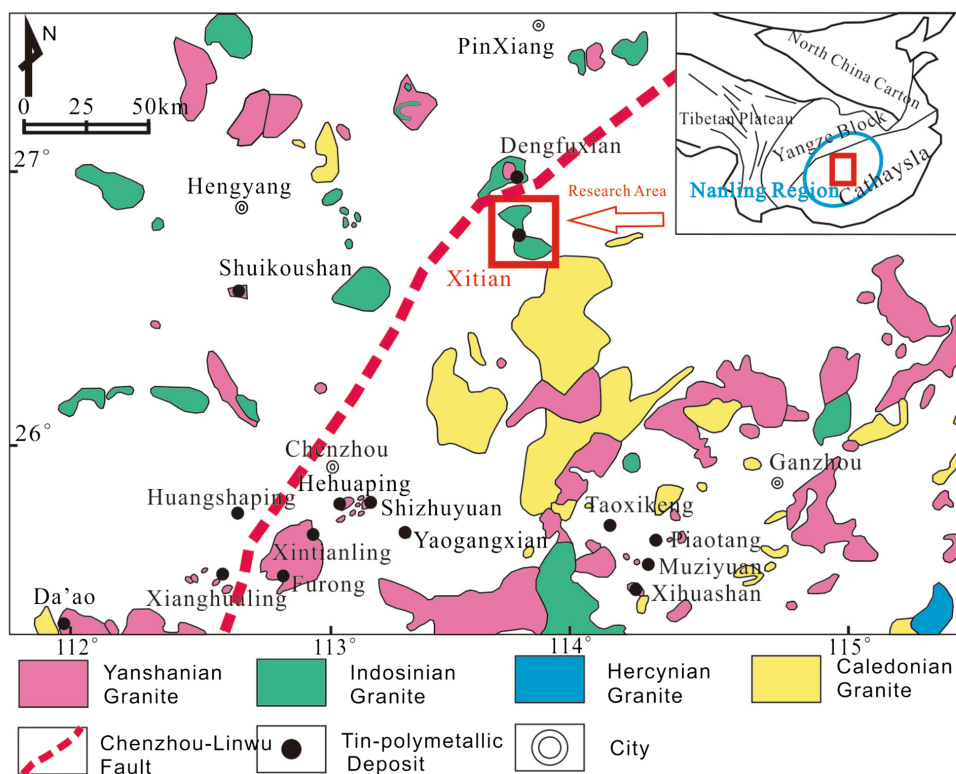
✉ Qing Liu  
qingliu@ucas.ac.cn

<sup>1</sup> Key Laboratory of Computational Geodynamics, Chinese Academy of Sciences, Beijing 100049, China

<sup>2</sup> College of Earth Science, University of Chinese Academy of Sciences, Beijing 100049, China

<sup>3</sup> 416 Geological Team, Bureau of Geology and Mineral Exploration and Development of Hunan Province, Zhuzhou 412007, China

**Fig. 1** Simplified geological map of central Nanling Range, South China, and the distribution of mineral deposits. Modified after Sun (2006)



lithology (Niu et al. 2015). Rocks of similar petrography have different ages, which hamper the ability for age determination. Previous studies on the Xitian deposit mainly focused on the ages of a certain type of mineralization (Fu et al. 2012; Liu et al. 2008a; Ma et al. 2008). Without considering the different types of the mineralization, these studies restricted the understanding of the metallogenesis in the Xitian deposit. Moreover, the mineralization in the Xitian composite pluton displays different types associated closely to the location, which means mineralization was developed at different locales with different occurrence in the Xitian composite pluton (Fu et al. 2009; Wu et al. 2009). To better understand the association between different types of mineralization and structures, it is important to investigate the architecture of faults combining with the forming time of mineralization. It is helpful to determine if and how different types of mineralization formed in a particular tectonic.

Common technique for direct dating of the mineral deposits is through using ore minerals. However, it is notoriously difficult to directly determine the age of mineralization because of the absence of suitable minerals for dating by conventional techniques. In recent years, benefiting from the development of Multi-collector Laser Ablation Inductively Coupled Plasma Mass Spectrometry techniques (MC-LA-ICP-MS) and other instruments, in-situ U-Pb dating on zircon and other U-bearing accessory phases has made significant progress in obtaining precise

and accurate ages (Yuan et al. 2011). Direct U-Pb dating of rutile ( $TiO_2$ ) has been widely accepted. Owing to the similarity of the crystal structure of rutile, significant U content incorporated in the cassiterite lattice can be used to date the tin-bearing deposit (Gulson and Jones 1992; Liu et al. 2007; Yuan et al. 2007). Additionally, theoretical studies on the closure temperature and dynamics of diffusion reveal that cassiterite can preserve the original U-Pb isotope system under high temperatures (Zhang et al. 2011). Therefore, cassiterite should offer the same advantages as rutile for the direct dating of mineral deposits. U-Pb dating on cassiterite by isotope dilution thermal ionization mass spectrometry (ID-TIMS) and LA-MC-ICP-MS has demonstrated that cassiterite is a robust candidate for U-Pb dating of tin-polymetallic mineralization (Yuan et al. 2011). Coupled with the studies on zircon, application of cassiterite U-Pb dating has provided data on the genetic relationship between the timing and genetic processes of related mineral deposits (Chen et al. 2013a, b; Li et al. 2013; Ma et al. 2013; Wang et al. 2014a, b; Zhang et al. 2014, 2015, 2017).

Above all, it is essential to confirm the time of skarn-type mineralization which spatially associated with the Indosinian granite. Research of structures combining the forming time of different types of mineralization provides the useful information for the geodynamic processes in the Xitian deposit, and by extension of the Nanling Range. To address this issue, systematic LA-MC-ICP-MS U-Pb

dating on cassiterite collected from the Xitian tin-polymetallic deposit were performed here. We combined the age of different types of mineralization with the structural signatures to understand the genetic link between the structures and mineralization.

## 2 Geological setting

The Xitian deposit is located in the central of the Nanling Range, which hosts numerous W–Sn deposits associated with several cycles of polygenetic granitic intrusions (Hu and Zhou 2012; Mao et al. 2013; Zhao and Zhou 2015). It lies in the western part of the Cathaysia Block (Fig. 1), which is one piece of the South China Block (Zhao et al. 2011). The Xitian tin-polymetallic deposit, located in the margin of the Xitian granite in eastern Hunan Province, is one of the large-scale tin-polymetallic deposits in the central part of the Nanling Range in Cathaysia Block (Fig. 1).

### 2.1 Sedimentary rocks

The exposed strata in the Xitian deposit include Ordovician sandstones, Middle and Upper Devonian carbonate rocks, Carboniferous carbonate rocks and Cretaceous red beds, all of which are partly unconformable overlain by Neogene clay rocks (Fig. 2). The Upper Devonian strata can be divided into two formations, the Xikuangshan and Shetianqiao. The Xikuangshan Formation is up to 300 m

thick and consists of quartz sandstone and shales. The Shetianqiao Formation is thinly layered and predominantly composed of quartz sandstones. The Middle Devonian strata mainly consist of the Qiziqiao Formation in the Xitian deposit, which is primarily made up of dolomite, dolomitic limestone, and limestone. The Qiziqiao Formation is the host rock of most W–Sn–Pb–Zn deposits in this region (Yao et al. 2014).

### 2.2 Structure

The Xitian deposit is located in the eastern part of the NE-trending Chenzhou–Lingwu fault and close to the contact zone of the Xitian composite pluton (Fig. 1). The tectonic framework of this area mainly consists of a SN-trending extensional structure of granite dome, a series of NE-trending multiple folds, and NE trending strike-slip tectonic system (Wang and Zhang 2014; Wu et al. 2012b). The faults and inter-layer gliding zones between the Qiziqiao Formation and Xikuangshan Formation might promote the migration of the ore-forming fluids. The skarn-type mineralization in the Xitian deposit is predominately located at the anticlinal cores which consist of the Qiziqiao Formation dolomitic limestone overprinted by the granite. The strike-slip system controls the distribution of quartz-vein tin-polymetallic orebodies (Fig. 2). Multiple episodes of activity also result in numerous small-scale faults and folds (Ma et al. 2005; Wu et al. 2009; Xu et al. 2006).

**Fig. 2** Geological map of the Xitian deposit and distribution of orebodies. Modified after topographical geological map that edited by Bureau of Geology and Mineral Exploration and Development of Hunan Province

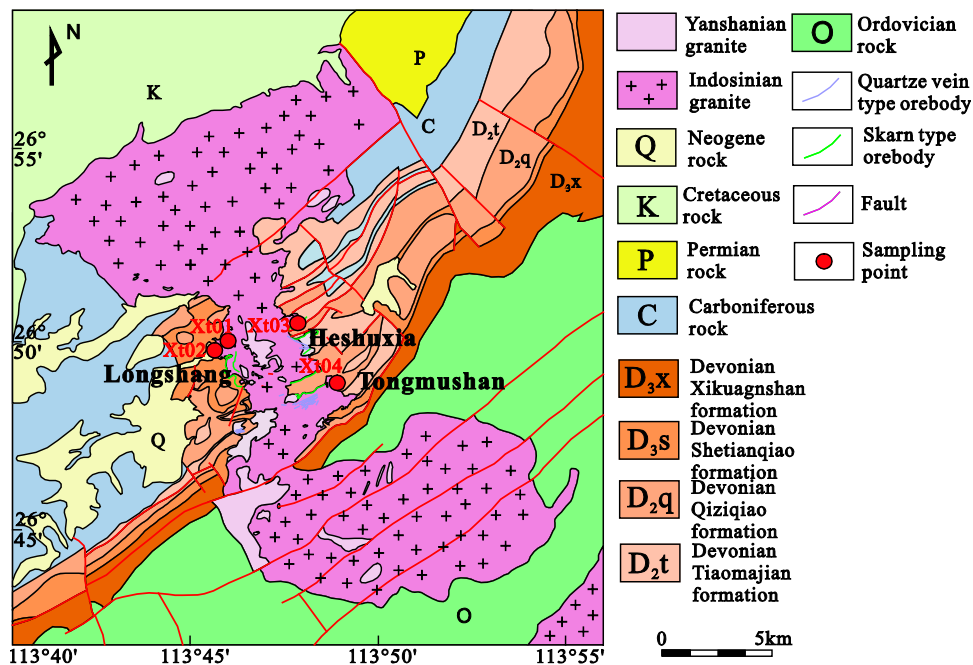


**Fig. 3** Field aspects and photographs of the main ore types from the Xitian deposit. **a** The mineralization type of quartz vein, **b** the mineralization type of skarn, **c** sample of quartz vein type, **d** sample of skarn type, **e** zonal texture of cassiterite from the quartz type, **f** cassiterite is accompanied with scheelite, sphalerite, galena, **g** the character of biotite granite in the transmission light, **h** the character of porphyreous biotite monzogranite in the transmission light. *Q* quartz, *Cst* cassiterite, *Sch* scheelite, *Sp* sphalerite, *Gn* galena, *Bi* biotite, *Kfs* K-feldspar, *Pl* plagioclase

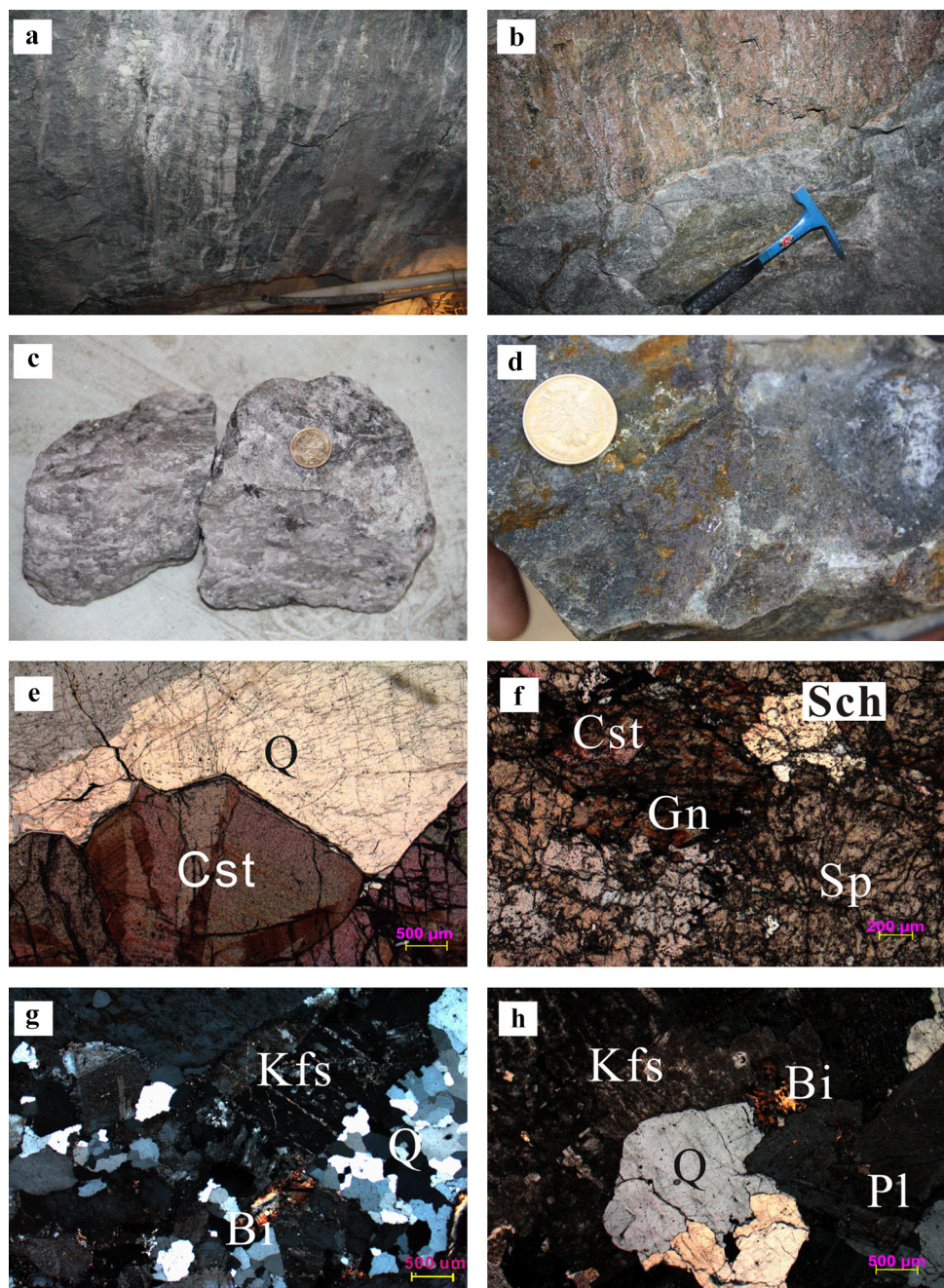


**Table 1** The standard information of samples

	Group one			Group two		
Type of mineralization	Quartz vein			Skarn		
Sample	2510	2616	2827	2710	2820	2824
Location	Xt01	Xt04	Xt02	Xt03	Xt02	Xt02
Age of granite (Ma)	$232.4 \pm 2.3$	$232.6 \pm 2.1$	$232.0 \pm 1.8$	$153.6 \pm 1.4$	$232.0 \pm 1.8$	$232.0 \pm 1.8$

### 2.3 Igneous rocks

The Xitian deposit is located along the margin of the Xitian composite pluton, which mainly intrudes into Devonian strata with an outcrop area of ca 230 km<sup>2</sup>. The Xitian composite pluton is mainly of biotite granite, and porphyreous biotite monzogranite. The granites can be divided into two episodes by geochronological data, that is, the late Triassic (ca. 230 Ma) and the Late Jurassic (ca. 150 Ma) (Fu et al. 2009; Ma et al. 2005; Niu et al. 2015). The Late Triassic granite mainly crops out along the core and northern part of the Xitian composite pluton. The Late Jurassic granite only occurs in the inner part of the pluton and along the eastern orebody (Fig. 2). The Xitian composite pluton is comprised of massive biotite granite with granitic texture, consisting of 35vol%–40vol% quartz, 30vol%–36vol% K-feldspar, 20vol%–25vol% lagooclase, 5vol%–7vol% biotite (Fig. 3g). The porphyreous biotite monzogranite is characterized by 10vol%–15vol% phenocrysts consisting of almost K-feldspar and matrix containing 30vol%–35vol% quartz, 30vol%–35vol% K-feldspar, 25vol%–30vol% plagioclase, 5vol%–6vol% biotite (Fig. 3h). The dark microgranular enclaves were discovered in the Late Jurassic granite and have plastic shape and magmatic structure (Chen et al. 2014).

### 2.4 Mineralization

The ore veins are mainly hosted in granite and in the contact zone between the granite and Devonian carbonate rocks. It is obvious that the ore veins are controlled by the faults in the area. So far, more than 14 ore-veins have been explored in the Xitian deposit, and these are mainly distributed in Longshang, Heshuxia and Tongmushan (Xu et al. 2006). Two predominant mineralization types have been recognized as skarn and quartz vein (Fig. 3a, b). The majority of the orebodies are skarn-type, with the most common ore minerals being cassiterite and scheelite, accompanied by minor amounts of magnetite, chalcopyrite, galena, and sphalerite. The gangue minerals are predominately quartz, feldspar, muscovite and diopside (Fig. 3d, f). The ore minerals are commonly anhedral to subhedral with metasomatic texture and banded structure. The quartz vein type ores are mainly distributed along the NE fractures, with the most common ore minerals being cassiterite, sphalerite and chalcopyrite with granular texture and disseminated structure. Accompanying the ore mineral, the gangue minerals predominately are quartz, feldspar, muscovite, fluorite and chlorite (Fig. 3c, e). The orebodies that lie in the western part of the granite which distribute in Longshang are mainly skarn types, while the vein-type are usually associated with the eastern portions of the granite distributed in Heshuxia and Tongmushan. The ore-bearing

quartz veins commonly, but not always, overlay above the skarn type orebodies (Fu et al. 2009; Wu et al. 2012b).

## 3 Methods

### 3.1 Sampling and preparation

In order to determine the accurate age of mineral deposit, six cassiterite samples were collected from different types of mineralization in the Xitian tin-polymetallic deposit. Samples 2510, 2616, and 2827 were from the quartz vein type ores, while samples 2710, 2820, and 2824 were from the skarn type ores. Most of the samples (2510, 2616, 2827, 2820, and 2824) were collected from the orebodies which lie in the contact zone between Indosinian granite and Devonian carbonate or in the interior part of Indosinian granite so as to figure out whether existing Indosinian mineralization (Table 1). The sample of 2710 was collected from the orebodies associated closely with Yan-shanian granites. The granites accompanied with mineralization in our study have been dated by measuring the U-Pb of zircon (Niu et al. 2015). To determine the relationship between mineralization and structure, we performed a mesoscopic structural analysis combined with systematically geochronology.

The preparation of samples for cassiterite dating was conducted in the Laboratory of the Institute of Geology and Mineral Resources, Langfang, Hebei Province, China. The samples were crushed into 40–60 mesh, and the cassiterite grains selected for U-Pb analysis were separated by standard mineral separation techniques and checked under the binocular microscope to ensure the absence of inclusions, surface alteration and fractures (Yuan et al. 2011). Cassiterites without inclusions and cracks, and of high optical quality were attached to a piece of slide with double-sided tape. Then, a PVC ring was placed on it with a mixture of epoxy and hardener. After totally solidifying, the ring was peeled off the slide and ground down to expose the interior portions of most grains. Before machine analysis, the sample surface was cleaned with ethanol and ultrapure water to eliminate surface contamination (Yuan et al. 2011).

### 3.2 Analytical techniques

Uranium and lead isotopes were analyzed by using a Thermo Fisher Neptune MS-ICP-MS coupled with a (ESI) UP193FX ArF Excimer Laser ablation system at the Tianjin Institute of Geology and Mineral Resources. The mass spectrometer includes a mass analyzer with double ion focusing and zoom optics, which enables the direct measuring of isotope ratios with a relative mass difference

**Table 2** U–Pb isotope data for cassiterite from quartz vein

2510				2616				2827			
$^{238}\text{U}/^{206}\text{Pb}$	Err%	$^{207}\text{Pb}/^{206}\text{Pb}$	Err%	$^{238}\text{U}/^{206}\text{Pb}$	Err%	$^{207}\text{Pb}/^{206}\text{Pb}$	Err%	$^{238}\text{U}/^{206}\text{Pb}$	Err%	$^{207}\text{Pb}/^{206}\text{Pb}$	Err%
23.49	1.07	0.40	1.42	39.67	0.98	0.06	3.79	38.57	1.11	0.10	4.97
40.51	0.95	0.05	2.41	36.60	0.99	0.13	2.15	39.98	1.16	0.08	7.05
39.22	1.00	0.09	3.74	31.34	1.39	0.20	4.24	40.00	1.00	0.05	5.97
18.00	2.66	0.65	3.90	39.39	0.99	0.09	2.97	36.66	1.61	0.09	13.53
40.69	0.96	0.06	2.99	41.15	1.04	0.07	6.52	37.04	1.46	0.10	8.82
21.21	1.60	0.46	1.76	38.18	1.28	0.10	5.87	40.15	1.29	0.06	10.92
36.12	0.97	0.16	1.73	40.16	0.96	0.08	2.23	39.47	1.31	0.05	18.10
1.58	1.88	0.88	1.23	41.22	0.95	0.05	2.31	22.03	1.43	0.39	2.02
32.75	1.13	0.21	2.79	39.04	1.46	0.07	14.07	35.69	1.10	0.15	3.04
19.28	1.06	0.51	1.29	39.79	1.07	0.05	9.48	40.56	1.01	0.07	4.57
40.63	0.98	0.07	3.92	39.92	1.09	0.07	7.49	36.43	2.65	0.08	17.30
21.40	1.11	0.45	1.44	35.05	1.06	0.16	3.05	37.34	1.26	0.12	6.05
37.24	0.98	0.13	2.01	40.54	1.51	0.09	11.79	39.16	1.36	0.07	12.19
4.94	1.01	0.81	1.22	38.19	1.15	0.08	8.25	40.61	1.39	0.07	10.97
28.83	0.98	0.31	1.36	40.41	0.97	0.06	3.77	38.18	1.51	0.10	9.71
15.72	1.84	0.56	1.64	39.05	1.29	0.08	10.04	38.61	1.54	0.12	7.81
25.36	1.02	0.38	1.40	40.64	1.02	0.05	7.54	35.21	2.34	0.16	17.26
10.31	2.17	0.70	1.43	31.67	1.22	0.24	2.56	30.37	2.15	0.23	9.30
27.47	1.10	0.33	1.52	37.07	1.20	0.12	5.02	37.73	1.30	0.06	12.93
13.64	1.03	0.62	1.23	40.75	0.97	0.06	3.52	38.21	1.24	0.07	10.09
41.28	1.01	0.06	5.26	37.66	1.48	0.11	8.64	38.43	3.34	0.27	16.07
36.76	0.99	0.15	2.30	37.06	1.02	0.11	2.99	33.74	7.65	0.27	16.34
40.44	0.94	0.08	1.63	35.17	0.97	0.17	1.69	36.31	1.31	0.15	4.60
16.51	1.15	0.56	1.32	39.14	1.08	0.08	6.62	33.49	3.01	0.22	20.55
40.71	1.05	0.08	5.71	24.27	1.41	0.40	2.15	39.54	1.22	0.08	7.55
41.56	0.98	0.05	4.66	37.59	1.29	0.12	7.14	40.90	1.01	0.06	5.55
15.83	1.07	0.59	1.28	39.87	1.00	0.08	3.48	38.16	1.87	0.11	14.09
37.66	1.08	0.13	4.35	40.65	1.05	0.06	5.93	39.14	1.27	0.09	8.08
40.93	1.07	0.05	9.91	40.28	0.94	0.06	1.48	33.54	3.06	0.19	18.53
37.63	0.97	0.13	2.06	40.89	1.64	0.13	10.03	30.05	2.35	0.20	12.21
9.69	2.80	0.82	8.34	35.91	1.26	0.15	5.56	27.53	2.43	0.33	6.89
34.51	1.40	0.16	6.19	40.35	0.95	0.05	2.87	37.16	1.21	0.13	4.85
13.77	1.04	0.63	1.39	38.54	1.05	0.11	3.42	37.89	1.20	0.16	4.33
35.89	0.99	0.16	2.09	40.76	0.96	0.06	2.88	30.29	1.27	0.25	2.98
11.84	0.99	0.67	1.24					30.01	1.37	0.25	3.52
40.78	0.95	0.06	2.25					36.23	1.37	0.13	5.76
41.89	0.96	0.04	4.13					30.71	1.52	0.23	4.30
41.10	1.25	0.07	11.28								
35.45	1.61	0.20	4.28								
36.68	1.30	0.12	5.23								
41.62	0.95	0.06	2.38								

of up to 17%. Helium was used as the carrier gas to transport the ablated material produced by the laser with an energy density of approximately 13–14 J/cm<sup>2</sup> at a flow rate of 8–10 Hz (Chen et al. 2014; Li et al. 2013; Yuan et al. 2011). To ensure the data collected was valuable and

accurate, cassiterites chosen to ablation had no inclusions and cracks.

In order to correct the instrument drift and mass bias, all the data for U–Pb analysis were corrected by the in-lab external standard sample (AY-4), which already had a

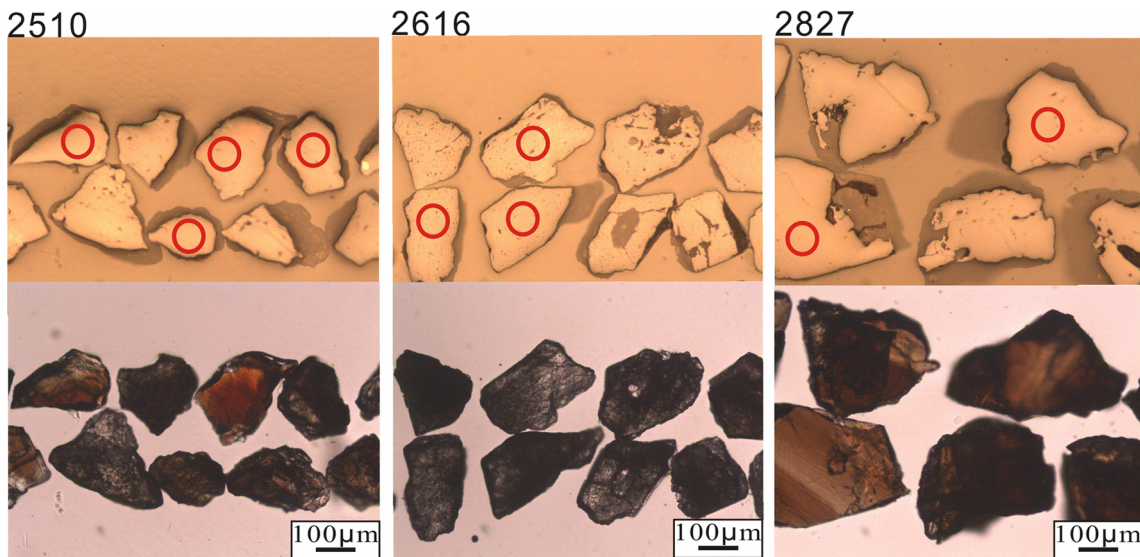


**Fig. 4** Transmission and reflected images of cassiterite from the quartz veins, Xitian deposit

well-determined U–Pb age by ID-TIMS. It was collected from the No. 19 skarn orebody in the Anyuan tin deposit of the Furong deposit in the Nanling Range (Yuan et al. 2007, 2011). To ensure the reliability of the measured results and then to monitor the stability of the instrument, the standard sample was measured after every two samples.

Considering the relatively high content of the common lead in cassiterite, the Tera–Wasserburg concordia diagram was preferred for U–Pb dating. Results obtained for closed systems plot were on the Concordia, whereas those obtained from open systems were discordant, which may define a discordant line whose intersections with the Concordia curve indicate the time of formation that of disturbance of the system (Li et al. 2016). Therefore, the low intersection point age of cogenetic samples in the Concordia diagram can represent the age of mineral crystallization. The age calculation and plotting Concordia diagrams was performed by using Isoplot (Ludwig 1994). The Tera–Wasserburg diagram is very useful for samples with substantial amounts of common Pb, especially for the data analyzed using LA-ICP-MS method (Li et al. 2016; Tera and Wasserburg 1972).

## 4 Results

### 4.1 U–Pb age of cassiterite

To evaluate the mineralization age, six samples from different types of mineralization were used for in-situ LA-MC-ICP-MS U–Pb analyses only. Three samples of group one from quartz vein type (2510, 2616, and 2827) were dated. The dataset is listed in Table 2. Most of the cassiterite crystals were light to dark brown, euhedral to subhedral, and

100–200  $\mu\text{m}$  in length (Fig. 4). Some coarse-grained cassiterite crystals displayed short prismatic figure.

Thirty-four analyses of sample 2616 were plotted at the intercept age of  $155.2 \pm 1.8$  Ma (MSWD = 2.5, Fig. 5b). Meanwhile, thirty-seven spots from the sample of 2827 yielded a U–Pb concordia lower intercept age of  $156.2 \pm 4.0$  Ma (MSWD = 3.1, Fig. 5c). Forty-one spots analyzes of sample 2510 yielded a U–Pb concordia lower intercept age of  $154.5 \pm 2.2$  Ma (MSWD = 1.8, Fig. 5a).

The U–Pb data for samples of group two from skarn type ores (2710, 2820, and 2824) are listed in Table 3. Comparing to group one, most cassiterite crystals were lighter and smaller. Majority shapes of crystals were 40–150  $\mu\text{m}$  in length in Fig. 6. Some coarse-grained cassiterite crystals have short prismatic or bipyramidal (Fig. 6).

Twenty spots were analyzed from the sample of 2710 of the group two and yielded a lower intercept age of  $154.5 \pm 4.3$  Ma (MSWD = 19, Fig. 7a). Data from sample of 2820 of the group two yielded was plotted at the intercept age of  $157.3 \pm 2.1$  Ma (MSWD = 5.9) with thirty-six spots (Fig. 7b). Forty-one spots from another sample of 2824 yielded a lower intercept age of  $155.9 \pm 1.6$  Ma (MSWD = 3.3, Fig. 7c).

In summary, the lower intercept age of cassiterite from the quartz vein ranged from 154 to 156 Ma. Meanwhile, the data of skarn type yielded a lower intercept age of  $154 \pm 4.3$ – $157.4 \pm 2.1$  Ma. All six samples displayed a relatively narrow range of U–Pb lower intercept ages varying from  $154.5 \pm 2.2$  to  $156.2 \pm 4.0$  Ma. Obviously, although the type of mineralization was different, the ages of the ore-forming that were defined by our studied all fell into the range of 150–160 Ma when Sn-polymetallic mineralization occurred widely in the Nanling Range.

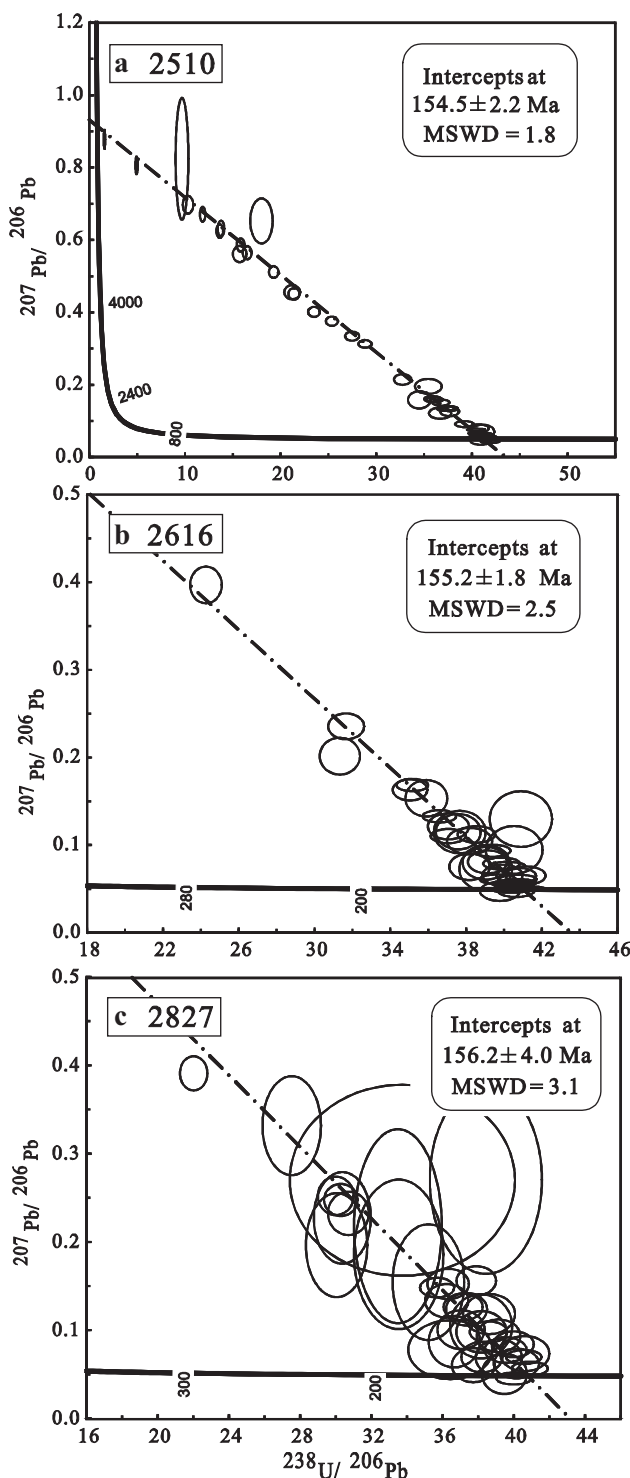


**Fig. 5** The U–Pb corresponding concordia diagram (a–c) of cassiterite from quartz veins, Xitian deposit

#### 4.2 Structural signatures

Kinematic indicators can be defined as structures developed at shear zone boundaries and within shear zones that are asymmetric with respect to both the boundaries and any

foliation developed within the zones (Behrmann 1987; Hancock and Barka 1987). A diverse assemblage of kinematic indicators can tell the direction and sense of shearing. Shear orientations measured in the Xitian deposit are plotted in Fig. 2.

The lineations and T fractures were directly observed in the place where the sample (2510) of quartz vein type were collected (Fig. 8a). The lineations extended along the east–west direction and these fractures developed in granite along the shear zone (Fig. 8b). The quartz veins formed in echelon arrays along brittle shear fractures. This means that the extension fractures were parallel to one other but offset from one another along the trend of the shear fracture, which was oblique to the extension fracture plane (Lafrance 2004). The occurrence of the quartz veins was unstable and did not extend far, indicating the signatures of T fracture (Fig. 8c). The veins penetrated the fault surface dipping 45° down-slope, and their dimensions ranged from few centimeters to meters.

On the place where samples (2820, 2824, 2827) were collected, strain fractures were abundant (Fig. 9a). The mineralization of skarn type was formed in the upper of the shear zone where it is in contact with the carbonate (Fig. 9b). The minor fractures in the shear zone displayed the geometry of Riedel shear. They developed along the fault surface with an angle of 15° (Fig. 9c). In the shear zone, the development of a series of R joints was facilitated by the magma–tectonic system activity. The joints presented as the quartz veins and their width were stable.

All these kinematic indicators suggest the involvement of a sinistral shear component along these shear zones. It means different types of mineralization were developed in the same tectonic system. Close to the place where sample (2710) was collected, the shear zone was developed along the bedding planes (Fig. 10a). The S-C fabrics indicated top-to-the-NE sense of shear in the east side of the granite (Fig. 10b). Combined to the NW sense of shear in the western parts of the granite, the fabrics displayed the characteristic of the deformation caused by the granite dome. Together with the time of the mineralization, the data indicate that the deformation of the shear zone is accordance with the Yanshanian magmatic activity.

## 5 Discussions

### 5.1 Aging of two types of W–Sn mineralization

Crystal structure of cassiterite is a close analogue to that of rutile. The significant U contents make it a good candidate to date the tin-bearing mineral deposits directly (Gulson and Jones 1992). Additionally, the closure ability of the U–Pb isotope system in cassiterite had been studied to prove the

**Table 3** U–Pb isotope data for cassiterite from skarn type ores

2710				2820				2824			
$^{238}\text{U}/^{206}\text{Pb}$	Err%	$^{207}\text{Pb}/^{206}\text{Pb}$	Err%	$^{238}\text{U}/^{206}\text{Pb}$	Err%	$^{207}\text{Pb}/^{206}\text{Pb}$	Err%	$^{238}\text{U}/^{206}\text{Pb}$	Err%	$^{207}\text{Pb}/^{206}\text{Pb}$	Err%
39.40	1.19	0.06	8.96	38.57	0.96	0.07	2.25	39.20	0.98	0.06	3.86
40.35	1.18	0.06	9.27	37.35	1.02	0.12	2.65	35.73	1.00	0.14	2.37
27.59	1.15	0.23	2.45	36.66	0.98	0.08	1.57	37.07	1.03	0.13	2.74
35.29	1.95	0.12	15.44	34.84	1.15	0.08	5.31	37.39	0.95	0.13	1.56
39.69	0.97	0.06	1.65	35.00	1.11	0.17	3.26	34.52	1.35	0.17	5.11
10.45	0.99	0.51	1.25	38.20	1.43	0.08	13.16	38.27	1.04	0.15	1.37
28.09	1.07	0.18	1.70	33.10	1.47	0.19	4.95	40.54	0.98	0.07	3.34
26.46	1.47	0.21	2.70	33.78	3.88	0.11	8.53	33.19	1.12	0.22	2.46
34.25	0.99	0.14	2.32	31.01	2.50	0.26	8.27	31.32	1.14	0.22	2.39
44.05	1.02	0.07	4.75	40.09	1.32	0.09	8.35	37.41	0.95	0.12	1.43
40.42	1.00	0.06	4.46	39.84	1.03	0.06	6.17	34.54	1.17	0.18	3.05
39.16	0.96	0.07	2.69	30.59	1.23	0.27	2.52	41.25	0.94	0.05	1.84
34.67	1.06	0.16	2.63	29.55	1.11	0.29	2.09	31.24	1.07	0.26	1.72
18.17	1.52	0.32	3.10	39.93	0.94	0.07	1.75	39.09	0.97	0.10	2.74
38.76	1.10	0.06	7.98	22.55	1.93	0.41	3.30	39.78	0.96	0.08	2.10
35.25	1.52	0.11	7.35	40.14	0.95	0.08	1.80	39.48	0.99	0.08	4.44
35.41	1.21	0.21	3.19	39.83	0.95	0.07	2.18	29.85	1.07	0.29	2.01
27.26	1.22	0.29	1.76	40.13	0.97	0.07	3.04	31.51	1.05	0.24	2.15
36.47	1.16	0.08	6.36	27.35	1.83	0.30	5.79	39.41	1.08	0.11	2.84
18.42	1.04	0.31	1.65	25.43	1.49	0.34	2.30	39.70	0.97	0.08	3.02
39.89	1.11	0.08	7.31	8.71	1.57	0.70	1.42	31.99	1.10	0.27	1.94
29.84	1.02	0.23	1.88	40.13	0.95	0.07	1.91	39.72	1.15	0.10	6.25
26.91	1.54	0.19	2.07	28.96	1.70	0.26	3.74	38.90	0.99	0.10	3.17
40.36	0.98	0.06	4.40	40.38	1.11	0.06	8.85	27.78	1.16	0.33	1.69
40.06	1.00	0.06	4.68	37.58	1.27	0.11	4.62	35.10	1.03	0.15	2.67
31.38	1.02	0.18	1.64	40.23	0.95	0.06	1.88	40.17	0.94	0.06	1.52
35.53	0.99	0.15	2.02	32.06	1.75	0.19	8.44	38.42	0.98	0.11	1.58
28.98	1.73	0.19	5.80	40.46	1.26	0.06	11.68	27.14	1.49	0.36	1.89
39.61	1.04	0.07	5.26	41.06	0.95	0.06	2.53	23.73	1.50	0.41	2.37
33.78	1.50	0.12	4.50	40.32	0.95	0.06	2.39	32.20	0.97	0.23	1.45
35.74	1.29	0.13	5.62	38.44	1.44	0.09	9.92	35.31	0.98	0.16	1.91
38.09	1.17	0.10	6.25	37.73	1.67	0.11	11.91	33.64	1.33	0.22	4.24
29.38	1.12	0.24	1.93	33.27	1.45	0.21	4.40	33.39	1.12	0.22	2.34
29.23	1.33	0.22	2.59	39.39	0.97	0.07	3.47	32.98	0.97	0.21	1.51
37.70	1.08	0.12	3.58	40.11	0.95	0.06	2.26	35.06	1.16	0.19	3.16
31.41	1.13	0.18	2.90	40.89	0.98	0.06	3.93	31.86	1.23	0.23	3.32
41.89	0.96	0.04	4.13					37.54	1.30	0.11	7.74
41.10	1.25	0.07	11.28					33.79	0.98	0.21	1.37
35.45	1.61	0.20	4.28					32.19	1.36	0.21	3.25
36.68	1.30	0.12	5.23					39.18	2.24	0.10	9.18
41.62	0.95	0.06	2.38					16.46	1.31	0.63	1.59

reliability for isotope dating in cassiterite. It revealed that the U–Pb closure temperature for the cassiterite with a grain size of 1  $\mu\text{m}$  is higher than 500 °C (Zhang et al. 2011). In the Xitian deposit, homogenization temperature of fluid

inclusions hosted in quartz and fluorite from the mineralization phase range between 90 and 380 °C in the ore-forming process (Yang et al. 2007), which is obviously lower than the closure temperature of the U–Pb system in micro-

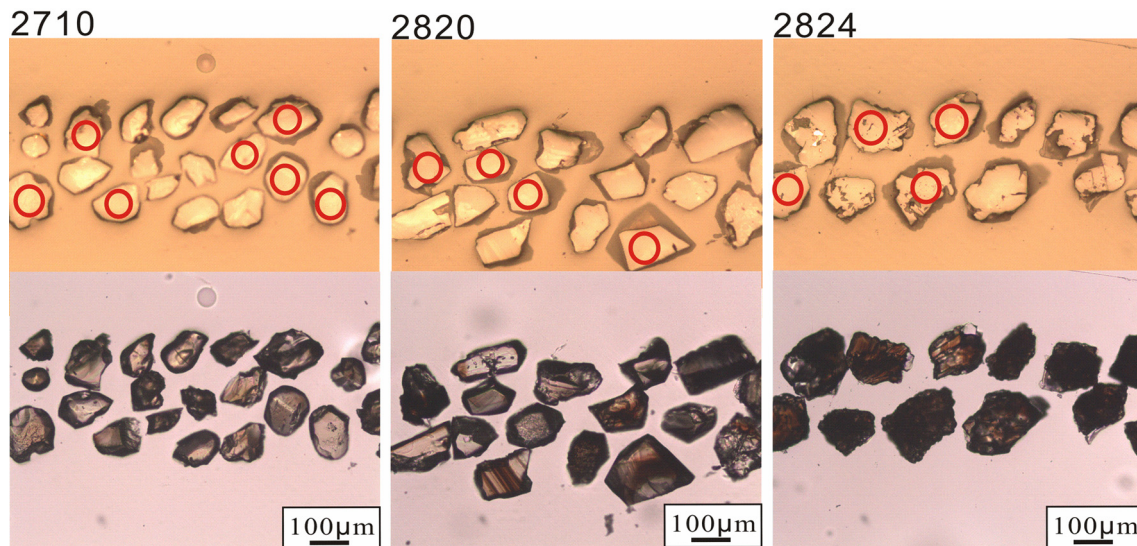


**Fig. 6** Transmission and reflected images of cassiterite from skarn type ores, Xitian deposit

grained cassiterite. Closure temperature will grow with an increase of grain radius (Dodson 1973). Thus, these data indicate that the U–Pb isotope system in coarse-grained cassiterite from the Xitian deposit could remain easily closed. The cassiterites for dating in this study was grained in sizes of 10–200  $\mu\text{m}$  in length, all of which were free of surface alteration and inclusions, indicating that the effective diffusion radii of this crystal is in excess of hundreds of microns (Zhang et al. 2014). All the above evidence could prove that the cassiterite had remained closed after mineral crystallization. In view of the reliable closure of the U–Pb system in cassiterite, the U–Pb age could be interpreted to represent the time of tin mineralization.

The Xitian tin-polymetallic deposit is spatially related to the Xitian granitoid intrusions which have been defined to multi-stages (Fig. 11). Field observations suggest that the skarn-type orebodies are located at the exo-contact zone of a coarse-grained granite intrusion with ages of 227–233 Ma (Mao et al. 2013; Niu et al. 2015). Liu et al. (2016) obtained an Re–Os isochron age ( $225.5 \pm 3.6$ ) by measuring the molybdenite-bearing granites. The results present the possibility of Indosinian mineralization in the Xitian deposit. But coupled with our study, the ages of the Xitian deposit were mainly falling into the range between 157 and 155 Ma within errors (Fig. 11). It can be concluded that the mineralization event including both types of quartz vein and skarn in the Xitian area associates much closer to the granite that formed in the Late Jurassic. The magmatic-hydrothermal event does exist in Indosinian in the Xitian deposit. However, whether or not the event is strong enough for mineralization still needs further research. In the Nanling Range, the mineralization was tremendous in late Jurassic, but was scattered and small

scale in Triassic. The different scale of mineralization probably resulted from different tectonic environments.

From the aspect of geochemistry, two stages of magmatism have a similar characteristic. According to their low  $\epsilon\text{Hf(t)}$  values ( $-14.69$  to  $-7.43$ ) and high  $\text{K}_2\text{O}$  contents, it suggests that they were mainly sourced from the re-melting of ancient granitoids (Zhou et al. 2015). Furthermore, together with the extensive existence of mafic enclaves, it indicates that the mantle-derived components were probably inputted into their sources in Yanshanian (Chen et al. 2014; Liu et al. 2008a). The petrography and geochemistry of the enclaves indicate that it was probably derived from quenching the mafic magma during its intrusion into felsic magma. Additionally, the zircons U–Pb data demonstrate that the age of enclaves is  $145.09 \pm 0.63$  Ma which is consistent with the Yanshanian granite (Chen et al. 2014). He and Ar isotopic components of fluid inclusions in pyrites from the main tin deposits in the central Nanling Range (including the Xitian deposit) indicate that the metallogenic fluids underwent significant mantle–crust derived fluids (Hu and Zhou 2012). The addition of mantle source material might be the critical factor of Sn-polymetallic mineralization. In the Nanling Range, all available data of extensive mantle–crustal interactions were responsible for the occurrence of extensive Sn-polymetallic mineralization in 150–160 Ma (Guo et al. 2011). Li and Li (2007) consider the Jurassic granite formed during a major igneous event in response to foundering of an early Mesozoic subducted flat-slab beneath SE China continent (Li et al. 2007; Li and Li 2007). The granites were likely generated through extensive fractional crystallization of mantle-derived alkaline parental magma associated with crustal assimilation (Li et al. 2007).

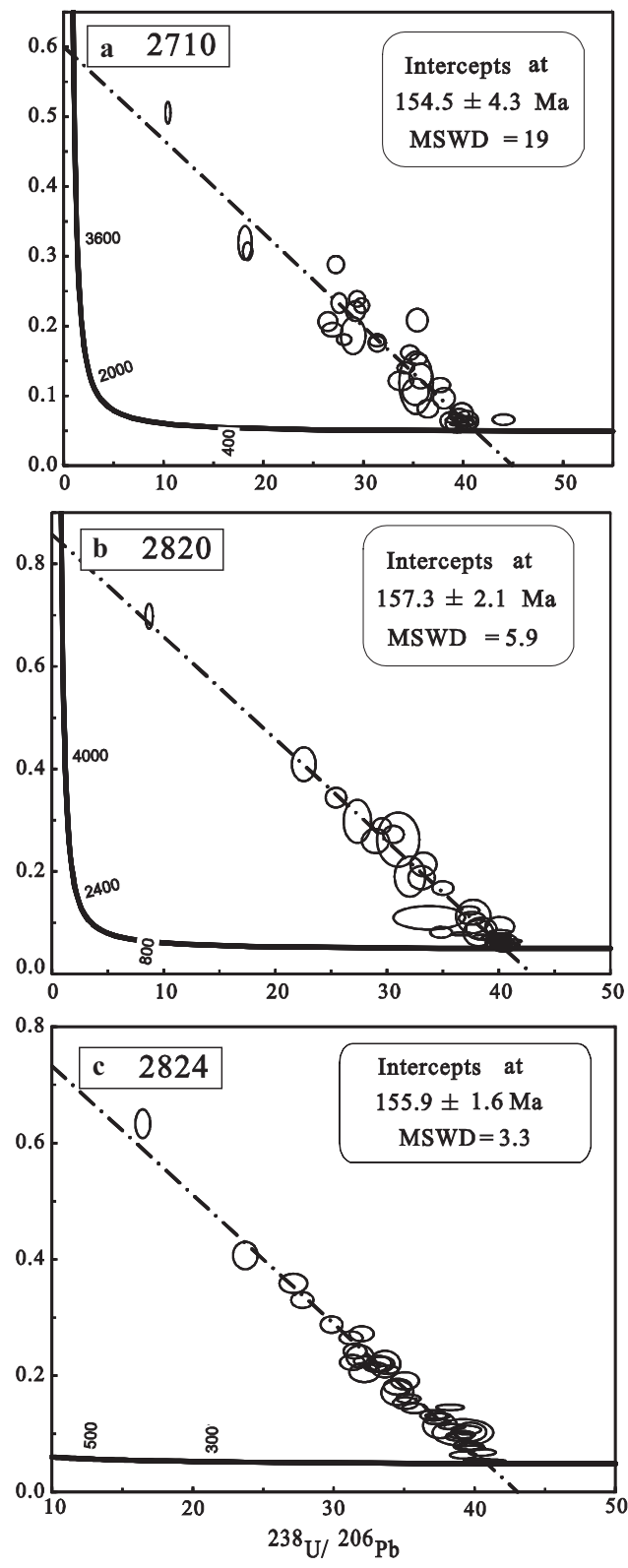


**Fig. 7** The concordia diagram (a–c) of cassiterite from skarn orebodies, Xitian deposit

## 5.2 Genetic relationship between the structure and mineralization

Considering the samples of cassiterite for the U–Pb dating were collected from the same point with the research of structures, it means different types of mineralization were developed in the same tectonic system. Plimer (1987) researched the behavior of the exsolved aqueous fluid is related to the internal overpressure ( $P_{in}$ ), the principal minimum shear ( $\sigma_3$ ), and the tensile strength of the rocks ( $t$ ). The aqueous fluid fractures the carapace and overlying rocks (i.e.  $P_{in} > \sigma_3 + t$ ) to form a vein system. Otherwise, the aqueous fluid fractures the carapace or ascends structures and interacts with porous, permeable, reactive rocks to form a skarn deposit (Plimer 1987). The Xiangdong tungsten deposit provides a vivid example of structure controlled ore forming processes in which the high-pressure fluid caused increasing local strain and reduced rock strength led to the development of a series of brittle fractures in the shear zone (Song et al. 2016). In conclusion, different types of mineralization in the Xitian deposit are coincidentally in the same magmatic–tectonic system, revealing that the contrasting style of mineralization is not specific to a particular tectonic setting. It depends on emplacement level, melt chemistry, distribution of the wall rocks, and more importantly, the structural control of the wall rocks (Romer and Kroner 2016).

While the mesoscopic structures indicate a sinistral shear in the western part of the Xitian granite, they indicate an opposite orientation of the shear zone in the eastern part. Based on the relationship to the geochronology, the radial deformation that is similar to the granite dome in the Xitian deposit may be caused by the magmatic intrusion. Granite domes in the Nanling Range are common and critical to the W–Sn mineralization. The architecture of the dome played an important role in controlling mineralization during a significant deviation in the maximum contractional stress vector to an east–southeast–west–southwest orientation (Chen et al. 2013b). The development of a pressure-quenched subsolidus carapace in the apical portion of a cupola is considered fundamental for the formation of tin deposit (Plimer 1987). Considering the different types of mineralization formed in the same magmatic–tectonic system in the Xitian deposit, the change of pressure played an important role in forming of ore deposit. With the upwelling of the mantle-derived magma, the mantle fluid efficiently extracted the ore element from magma on account of the special properties (Shervais and Jean 2012; Liu et al. 2012). Cavity expansion generated extreme reductions in pressure that caused the fluid to flow towards

**Fig. 8** The sketch of the structural signatures in the spot (xt01) where samples for dating were collected. **a** The linations along the shear zone, **b** the quartz vein strain as T fracture

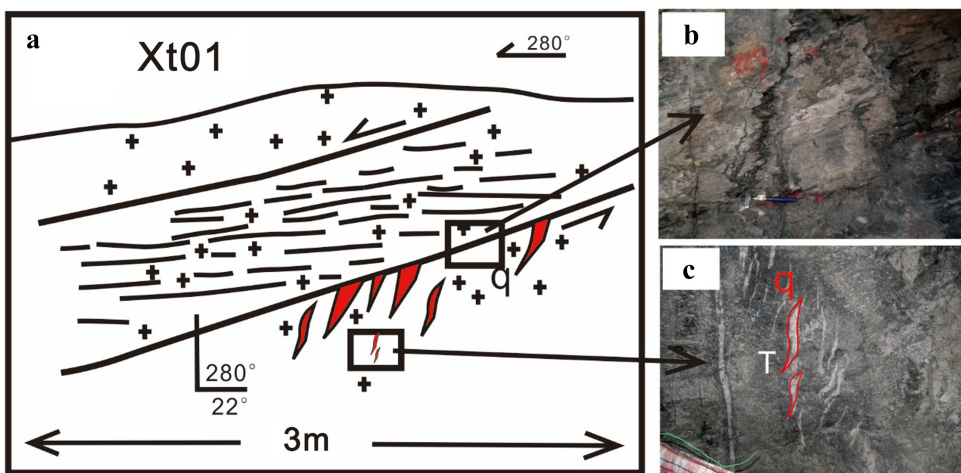


**Fig. 9** The sketch of the structural signatures in the spot (xt02) where samples for dating were collected. **a** The brittle fractures along the shear zone, **b** the quartz vein

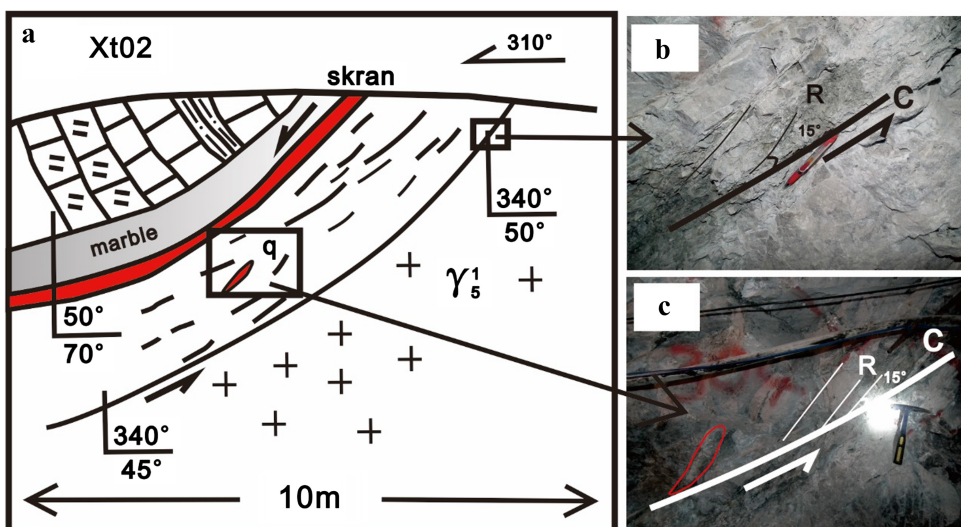
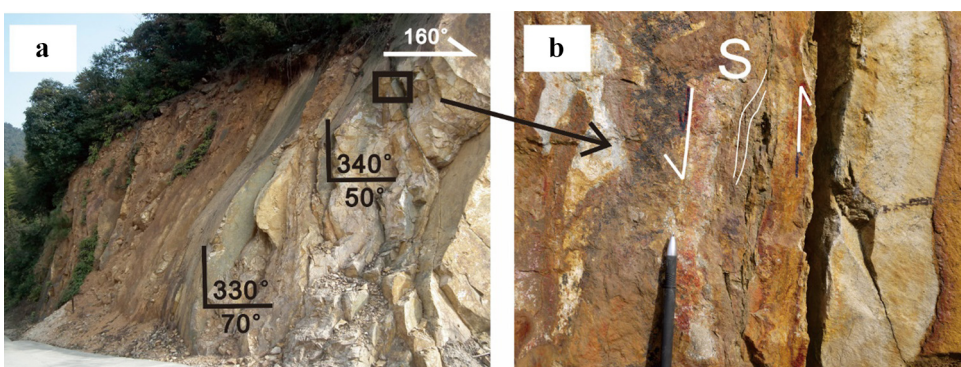


**Fig. 10** The photos of structural signatures in the western side of the granite (a) and S-C fabric (b)



and expand vapor. Such flash vaporization of the fluid resulted in the co-deposition of silica with a range of trace elements (Weatherley and Henley 2013). Different types of mineralization formed along the shear zone. The ore elements precipitated in different positions during the tectonic activity.

In the Nanling Range, the granite dome formation was closely related to some form of crust–mantle interaction (Chen et al. 2013a). Moreover, the Yanshanian mineralization was formed in an extensional setting (i.e.  $P_{in} > -\sigma_3 + t$ ), and the ore-forming elements in the magma could spread effectively with the liquids along faults and

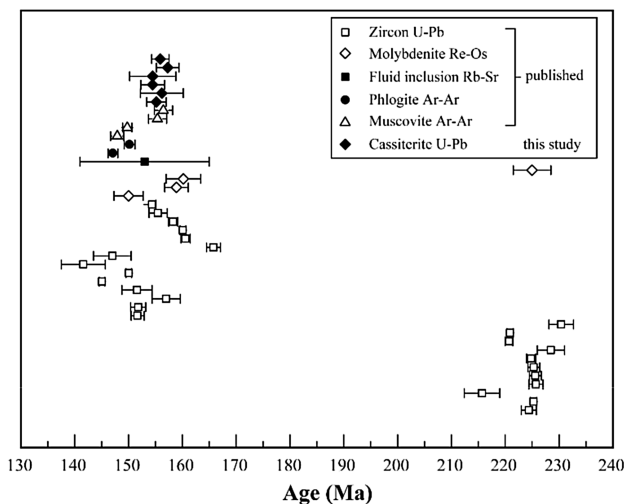


**Fig. 11** Age spectra of granitic magmatism and W–Sn mineralization in the Xitian deposit. Zircon U–Pb ages are from Chen et al. (2013a), Fu et al. (2009), Ma et al. (2005), Su et al. (2015), Yao et al. (2013) and Zhou et al. (2015). Molybdenite Re–Os ages are from Guo et al. (2014) and Liu et al. (2008a, b, 2016). Fluid inclusion Rb–Sr ages are from Fu et al. (2012). Phlogite Ar–Ar ages are from Su et al. (2015). Muscovite Ar–Ar ages are from Ma et al. (2008) and Su et al. (2015)

fractures (Bai et al. 2007; Plimer 1987). A subduction model was proposed based on the existing structural, geochronological, and sedimentary facies results. This model suggests that during the Mid-Jurassic (180–155 Ma), the full-scale slab foundering resulted in extensive magmatism that genetically associated with large-scale tin-polymetallic mineralization (Li et al. 2007; Li and Li 2007). Furthermore, ore deposit with certain characteristics of ore-forming elements, ore-controlling structures, spatial-temporal distributions, and related magmatic rocks are the response to their corresponding geodynamic framework.

## 6 Conclusions

1. The in-situ LA-MC-ICP-MS dating of cassiterite from different types of the Xitian tin-polymetallic deposits yielded a U–Pb concordia lower intercept age that ranged between 154 and 157 Ma. Combined with the granite that collected in the same spot, the tin-polymetallic mineralization that occurred in the contact of Triassic granite with the Devonian carbonate in the Xitian deposit was coincident with the emplacement of the late Jurassic of granite batholith. The U–Pb data in this study provides a temporal link between the late Jurassic magmatism and different types of tin-polymetallic mineralization, which possibility suggests the response of the foundering of a subducted flat-slab.

Additionally, the difference of tectonic settings might be one of the principal factors causing the metallogenetic difference between the Indosinian and Early Yanshanian granites in the Nanling Range.

2. The structure signatures where samples were collected for dating display the same characteristics. Combining with the age of different type of mineralization, these signatures indicate that the structural control of the wall rocks constrains the types of mineralization. Considering the structure in the district, granite dome plays an important role in the ore-forming process. The granite dome formation is closely related to some form of crust–mantle interaction. Additionally, ore deposit with certain characteristics of ore-forming elements, ore-controlling structures, spatial–temporal distributions, and related magmatic rocks are the response to their corresponding geodynamic framework.

**Acknowledgements** The authors give thanks to the Institute of Mineral Resources, Chinese Academy of Geological Sciences where all the experiments have been taken. We would like to thank Hui Li and other colleagues from 416 Brigade, Bureau of Geology and Mineral Exploration and Development of Hunan Province for their help during fieldwork. We also thank Dr. Guoxue Song and Wei Wei for their constructive suggestions on the manuscript. This work was financially supported by the Public Welfare Project of the Ministry of Land and Resources of China (201211024-04), National Key R&D Program of China (2016YFC0600401), National Science Foundation of China (NSFC Grant 41273046) and Research Cooperation between Institute and University of Chinese Academy of Sciences Grant (Y552012Y00).

## References

- Bai DY, Jia BH, Li JD, Wang XH, Ma TQ, Zhang XY, Chen BH (2007) Important significance of regional tectonic regime to metallogenetic capacity of Indosinian and Early Yanshanian granites in southeastern Hunan: a case study of Qianlshan and Wangxianling plutons. Miner Depos 26(5):487–500 (**in Chinese with English abstract**)
- Behrmann JH (1987) A precautionary note on shear bands as kinematic indicators. J Struct Geol 9(5):659–666
- Cai MH, Chen KX, Qu WJ, Liu GQ, Fu JM, Yin JP (2006) Geological characteristics and Re–Os dating of molybdenites in Hehuaping tin-polymetallic deposit, southern Hunan Province. Miner Depos 25(3):263–268 (**in Chinese with English abstract**)
- Chen D, Chen YM, Ma AJ, Liu W, Liu YR, Ni YJ (2013a) Magma mixing in the Xitian pluton of Hunan Province: evidence from petrography, geochemistry and zircon U–Pb age. Geol China 41(1):61–78 (**in Chinese with English abstract**)
- Chen J, Wang R, Zhu J, Lu J, Ma D (2013b) Multiple-aged granitoids and related tungsten-tin mineralization in the Nanling Range, South China. Sci China Earth Sci 56:111–121
- Chen XC, Hu RZ, Bi XW, Li HM, Lan JB, Zhao CH, Zhu JJ (2014) Cassiterite LA-MC-ICP-MS U/Pb and muscovite  $^{40}\text{Ar}/^{39}\text{Ar}$  dating of tin deposits in the Tengchong-Lianghe tin district, NW Yunnan, China. Miner Depos 49(7):843–860
- Dodson M (1973) Closure temperature in cooling geochronological and petrological systems. Contrib Miner Petrol 40(3):259–274

- Fu JM, Wu SC, Xu DM, Ma LY, Cheng SB, Chen XQ (2009) Constraint from Zircon SHRIMP U–Pb dating on the age of magma intrusion and mineralization in Xitian tungsten–tin polymetallic orefield, Eastern Hunan Province. *Geol Miner Resour South China* 3:1–7 (in Chinese with English abstract)
- Fu JM, Cheng SB, Lu YY, Wu SC, Ma LY, Chen XQ (2012) Geochronology of the greisen–quartz–vein tungsten–tin deposit and its host granite in Xitian, Hunan Province. *Geol Explor* 48(2):313–320 (in Chinese with English abstract)
- Gulson BL, Jones MT (1992) Cassiterite: potential for direct dating of mineral deposits and a precise age for the Bushveld Complex granites. *Geology* 20(4):355–358
- Guo C, Mao J, Bierlein F, Chen Z, Chen Y, Li C, Zeng Z (2011) SHRIMP U–Pb (zircon), Ar–Ar (muscovite) and Re–Os (molybdenite) isotopic dating of the Taoxikeng tungsten deposit, South China Block. *Ore Geol Rev* 43:26–39
- Guo CL, Li C, Wu SC, Xu YM (2014) Molybdenite Re–Os isotopic dating of Xitian deposits in Hunan Province and its geological significance. *Rock Miner Anal* 33(1):142–152 (in Chinese with English abstract)
- Hancock PL, Barka AA (1987) Kinematic indicators on active normal faults in Western Turkey. *J Struct Geol* 9(5–6):573–584
- Hu RZ, Zhou MF (2012) Multiple Mesozoic mineralization events in South China—an introduction to the thematic issue. *Miner Depos* 47:579–588
- Lafrance B (2004) Conjugate oblique-extension veins in shear and tensile fracture systems at the Komis gold mine and Mufferaw gold prospect, northern Saskatchewan. *Explor Min Geol* 13(1):129–137
- Li ZX, Li XH (2007) Formation of the 1300-km-wide intracontinental orogen and postorogenic magmatic province in Mesozoic South China: a flat-slab subduction model. *Geology* 35(2):179–182
- Li X, Li W, Li ZX (2007) On the genetic classification and tectonic implications of the Early Yanshanian granitoids in the Nanling Range, South China. *Chin Sci Bull* 52(14):1873–1885
- Li KW, Zhang Q, Wang DP, Cai Y, Liu YP (2013) LA-MC-ICP-MS U–Pb geochronology of cassiterite from the Bainiuchang polymetallic deposit, Yunnan Province, China. *Acta Miner Sin* 33(2):203–209 (in Chinese with English abstract)
- Li CY, Zhang RQ, Ding X, Ling MX, Fan WM, Sun WD (2016) Dating cassiterite using laser ablation ICP-MS. *Ore Geol Rev* 72:313–322
- Liu YP, Li ZX, Li HM, Guo LG, Xu W, Ye L, Li CY, Pi DH (2007) U–Pb geochronology of cassiterite and zircon from the Dulong Sn–Zn deposit: evidence for cretaceous large-scale granitic magmatism and mineralization events in southeastern Yunnan Province, China. *Acta Petrol Sin* 967–976 (in Chinese with English abstract)
- Liu GQ, Wu SC, Du AD, Fu JM, Yang XJ, Tang ZH, Wei JQ (2008a) Metalligenic ages of the Xitian tungsten–tin deposit, eastern Hunan Province. *Geotecton Mentallogenesis* 32(1):63–71 (in Chinese with English abstract)
- Liu S, Wang D, Chen Y, Li J, Ying L, Xu J, Zeng Z (2008b)  $^{40}\text{Ar}/^{39}\text{Ar}$  ages of muscovite from different types tungsten-bearing quartz veins in the Chong-Yu-You concentrated mineral area in Gannan region and its geological significance. *Acta Geol Sin* 82(7):932–940 (in Chinese with English abstract)
- Liu X, Li C, Lu Q, Deng B, Song X, Zhao F, Chu Y, Xiao J, Yi L, Huang Y (2012) The genesis mechanism of the mantle fluid action and evolution in the ore-forming process: a case study of the Laowangzhai gold deposit in Yunnan, China. *Acta Geol Sin (Engl Ed)* 86(3):608–618
- Liu D, Yang L, Deng X, Dai X, Wang X, Chong K, Du G, Wei H (2016) Re–Os isotopic data for molybdenum from Hejiangkou tungsten and tin polymetallic deposit in Chenzhou and its geological significance. *J Cent South Univ* 23:1071–1084
- Ludwig KR (1994) ISOPLOT: a plotting and regression program for radiogenic-isotope data; version 2.53. Open-file Report, 91
- Ma TQ, Bai DY, Kuang J, Wang XH (2005) Zircon SHRIMP dating of the Xitian granite pluton, Chaling, southeastern Hunan, and its geological significance. *Geol Bull China* 24(5):415–419 (in Chinese with English abstract)
- Ma LY, Fu JM, Wu SC, Xu DM, Yang XJ (2008)  $^{40}\text{Ar}/^{39}\text{Ar}$  isotopic dating of Longshang tin-polymetallic deposit, Xitian orefield, eastern Hunan. *Geol China* 35(4):706–713 (in Chinese with English abstract)
- Ma N, Deng J, Wang QF, Wang CM, Zhang J, Li GJ (2013) Geochronology of the Dasongpo tin deposit, Yunnan Province: evidence from zircon LA-ICP-MS U–Pb ages and cassiterite LA-MC-ICP-MS U–Pb age. *Acta Petrol Sin* 29(4):1223–1235 (in Chinese with English abstract)
- Mao JW, Xie GQ, Guo CL, Yuan SD, Cheng YB, Chen YC (2008) Spatial-temporal distribution of Mesozoic ore deposits in South China and their metallogenic settings. *Geol J China Univ* 14(4):510–526 (in Chinese with English abstract)
- Mao J, Cheng Y, Chen M, Franco P (2013) Major types and time-space distribution of Mesozoic ore deposits in South China and their geodynamic settings. *Miner Depos* 48:267–294
- Niu R, Liu Q, Hou QL, Sun JF, Wu SC, Zhang HY, Guo QQ, Wang Q (2015) Zircon U–Pb geochronology of Xitian granitic pluton in Hunan Province and its constraints on the metallogenic ages of the tungsten–tin deposits. *Acta Geol Sin* 31(9):2620–2632 (in Chinese with English abstract)
- Peng J, Zhou M, Hu R, Shen N, Yuan S, Bi X, Du A, Qu W (2006) Precise molybdenite Re–Os and mica Ar–Ar dating of the Mesozoic Yaogangxian tungsten deposit, central Nanling district, South China. *Miner Depos* 41:661–669
- Plimer IR (1987) Fundamental parameters for the formation of granite-related tin deposits. *Geol Rundsch* 76(1):23–40
- Romer RL, Krone U (2016) Phanerozoic tin and tungsten mineralization—tectonic controls on the distribution of enriched protoliths and heat sources for crustal melting. *Gondwana Res* 31:60–95
- Shervais JW, Jean MM (2012) Inside the subduction factory: modeling fluid mobile element enrichment in the mantle wedge above a subduction zone. *Geochim Cosmochim Acta* 95(11):270–285
- Song C, Wei W, Hou QL, Liu Q, Zhang HY, Wu SC, Zhu HF, Li H (2016) Geological characteristics of the Laoshan’ao shear zone and its relationship with the Xiangdong tungsten deposit, Chaling, eastern Hunan Province. *Acta Petrol Sin* 32(5):1571–1580 (in Chinese with English abstract)
- Su H, Guo C, Wu S, Hou K, Zhang Y (2015) Magma-hydrothermal fluid activity duration and material sources in the Xitian Indosinian–Yanshanian Complex. *Acta Geol Sin* 89(10):1853–1872 (in Chinese with English abstract)
- Sun T (2006) A new map showing the distribution of granites in South China and its explanatory notes. *Geol Bull China* 25(3):332–335 (in Chinese with English abstract)
- Tera F, Wasserburg GJ (1972) U–Th–Pb systematics in three Apollo 14 basalts and the problem of initial Pb in lunar rocks. *Earth Planet Sci Lett* 14(3):281–304
- Wang DS, Zhang HY (2014) Discussion on faults, tungsten–tin anomaly and ore-controlling factors of Chaling Area, Southeastern Hunan. *Geoscience* 28(6):1225–1233
- Wang XJ, Liu YP, Miao YL, Bao T, Ye L, Zhang Q (2014a) *In-situ* LA-MC-ICP-MS cassiterite U–Pb dating of Dulong Sn–Zn polymetallic deposit and its significance. *Acta Petrol Sin* 30(3):867–876 (in Chinese with English abstract)
- Wang ZQ, Chen B, Ma XH (2014b) *In-situ* LA-ICP-MS U–Pb age and geochemical data of cassiterite of the Furong tin deposit, the Nanling Range: implications for the origin and evolution of the

- ore-forming fluid. Sci China Press 59:2505–2519 (in Chinese with English abstract)
- Weatherley DK, Henley RW (2013) Flash vaporization during earthquakes evidenced by gold deposits. Nat Geosci 6(4):294–298
- Wu SC, Hong QH, Long WP, Luo Y (2009) Geological features and metallogenetic model of Xitian W–Sn polymetallic deposit, Hunan Province. Geol Miner Resour South China 2:1–6 (in Chinese with English abstract)
- Wu J, Liang HY, Huang WT, Wang CL, Sun WD, Sun YL, Li J, Mo JH, Wang XZ (2012a) Indosinian isotope ages of plutons and deposits in southwestern Miaoershan-Yuechengling, northeastern Guangxi and implications on Indosinian mineralization in South China. China Sci Bull 57:1024–1035
- Wu SC, Long ZQ, Xu HH, Zhou Y, Jiang Y, Pan CC (2012b) Structural characteristics and prospecting significance of the Xitian tin-tungsten polymetallic deposit, Hunan Province, China. Geotecton Metallog 36(2):217–226
- Xu HH, Wu SC, Yu YC, Xie YL, Long WP (2006) Geological characteristics and ore-controlling factors of Xitian skarn-type W–Sn deposit in Hunan Province. Geol Miner Resour South China 2:37–42 (in Chinese with English abstract)
- Yang XJ, Wu SC, Fu JM, Huang HL, Chang HL, Liu YH, Wei JQ, Liu GQ, Ma LY (2007) Fluid inclusion studies of Longshang tin-polymetallic deposit in Xitian ore field, eastern Hunan Province. Miner Depos 26(5):501–511 (in Chinese with English abstract)
- Yang F, Li XF, Feng ZH, Bai YP (2009)  $^{40}\text{Ar}/^{39}\text{Ar}$  dating of muscovite from greisenized granite and geological significance in Limu tin deposit. J Guilin Univ Technol 29(1):21–24 (in Chinese with English abstract)
- Yao Y, Chen J, Lu JJ, Zhang RQ (2013) Geochronology, Hf isotopic compositions and geochemical characteristics of Xitian A-type granite and its geological significance. Miner Depos 32(3):467–488 (in Chinese with English abstract)
- Yao Y, Chen J, Lu J, Wang R, Zhang R (2014) Geology and genesis of the Hehuaping magnesian skarn-type cassiterite-sulfide deposit, Hunan Province, Southern China. Ore Geol Rev 58:163–184
- Yuan S, Peng J, Hu R, Li H, Shen N, Zhang D (2007) A precise U–Pb age on cassiterite from the Xianghualing tin-polymetallic deposit (Hunan, South China). Miner Depos 43:375–382
- Yuan S, Peng J, Hao S, Li H, Geng J, Zhang D (2011) *In-situ* LA-MC-ICP-MS and ID-TIMS U–Pb geochronology of cassiterite in the giant Furong tin deposit, Hunan Province, South China: new constraints on the timing of tin-polymetallic mineralization. Ore Geol Rev 43:235–242
- Zhang DL, Peng JT, Hu RZ, Yuan SD, Zheng DS (2011) The closure of U–Pb isotope system in cassiterite and its reliability for dating. Geol Rev 57(4):549–554 (in Chinese with English abstract)
- Zhang D, Peng J, Coulson IM, Hou L, Li S (2014) Cassiterite U–Pb and muscovite  $^{40}\text{Ar}/^{39}\text{Ar}$  age constraints on the timing of mineralization in the Xuebaoding Sn–W–Be deposit, western China. Ore Geol Rev 62:315–322
- Zhang RQ, Lu JJ, Wang RC, Ping Y, Zhu JC, Yao Y, Gao JF, Li C, Lei ZH, Zhang WL, Guo WM (2015) Constraints of *in-situ* zircon and cassiterite U–Pb, molybdenite Re–Os and muscovite  $^{40}\text{Ar}/^{39}\text{Ar}$  ages on multiple generations of granitic magmatism and related W–Sn mineralization in the Wangxianling area, Nanling Range, South China. Ore Geol Rev 65:1021–1042
- Zhang RQ, Lu JJ, Lehmann B, Li CY, Li GL, Zhang LP, Guo J, Sun WD (2017) Combined zircon and cassiterite U–Pb dating of the Piaotang granite-related tungsten-tin deposit, southern Jiangxi tungsten district, China. Ore Geol Rev 82:268–284
- Zhao WW, Zhou MF (2015) *In-situ* LA-ICP-MS trace elemental analyses of magnetite: the Mesozoic Tengtie skarn Fe deposit in the Nanling Range, South China. Ore Geol Rev 65:872–883
- Zhao JH, Zhou MF, Yan DP, Zheng JP, Li JW (2011) Reappraisal of the ages of Neoproterozoic strata in South China: no connection with the Grenvillian orogeny. Geology 39:299–302
- Zhou Y, Liang X, Wu S, Cai Y, Liang X, Shao T, Wang C, Fu J, Jiang Y (2015) Isotopic geochemistry, zircon U–Pb ages and Hf isotopes of A-type granites from the Xitian W–Sn deposit, SE China: constraints on petrogenesis and tectonic significance. J Asian Earth Sci 105:122–139